Development of a Fused Deposition Modeling System to Build Form-Fit Joints Using an Industrial Robot

Maurice Schwicker
Department of Applied Engineering Sciences, University of Applied Sciences, Kaiserslautern, Kaiserslautern, Germany
Email: Maurice.Schwicker@hs-kl.de

Nikolay Nikolov
Technical University of Sofia, Strength of Materials Section, Sofia, Bulgaria
Email: nyky@tu-sofia.bg

***Abstract*—During the last years, Additive Manufacturing (AM) technologies have experienced substantial growth mostly due to their new design potentials. One technology commonly used in AM is Fused Deposition Modeling. Basically, virtual 3D models are segmented into a series of 2D cross-sections, which are then successively built on top of each other to create the final physical part. When implementing an industrial robot with additional rotational degrees of freedom to create these layers, new design possibilities are created. While layers no longer need to be parallel to the print bed and the final print may even leave the area above the print bed, it becomes possible to produce form-fit joints. In this article the development and commissioning of an Additive Robot Manufacturing System is shown, which is able to perform these tasks. Tests were conducted to confirm the feasibility of the approach.**

***Index Terms*—additive manufacturing, fused deposition modeling, fast filament fabrication, 3D printing, robotics, form-fit joint**

I. Introduction

The classical Fused Deposition Modelling (FDM) commonly referred to 3D Printing is widely spread and has become more and more useful not only for rapid prototyping but also for production of final parts [1]. This process has a lot of disadvantages, such as stair step effect, need for support structures, and strength issues [2–4]. Additionally, the 2½D Fused Deposition Modeling (FDM) approach causes some limitations to the details' shapes and part positioning within the build volume. That is why a lot of efforts are made to improve that technology. An efficient but challenging step is adding additional degree(s) of freedom (DOF) to the build process, paving the way from a 2½D to full 3D print process. This allows printing on an existing part to create form-fit joints. The easiest way to do this is to place an extruder onto an industrial robot (IR) arm. But a lot of hardware and software challenges arise [5–7]. Many attempts are described in literature, all of them being in research stage [8, 9]. No multi-DOF FDM solution with a corresponding slicer is making full use of all DOF's is available on the market This led to the decision to build an own Additive Robot Manufacturing System (ARMS). This system will be firstly used for test specimen production and for comparisons with conventional 2½D FDM technology after a prove of concept is realized.

II. Use of a Robotic Kinematic in an FDM Environment

A. New Process Parameters Due to Rotational DOF

An analysis of the FDM process characteristics and their interaction with the robotic kinematic influence factors has been provided in [9]. Starting with a state of research, the process specific challenges and the general feasibility are analyzed and verified.

Using an industrial robot (IR) to guide the nozzle, enables the kinematic flexibility of the FDM technology. Moreover, this approach extends the set of parameters which influence the modelling process – Fig. 1.

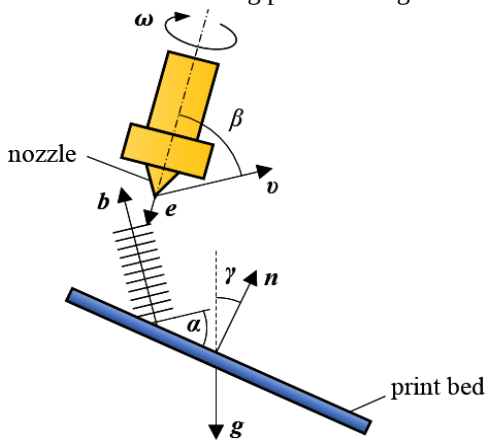

Figure 1. Basic geometrical relations of the FDM process (adapted from [9]).

Manuscript received June 7, 2021; revised November 1, 2021.

doi: 10.18178/ijmerr.11.2.51-58

The vectors, shown in Fig. 1 represent the basic geometric relations resulting from the kinematic flexibility. They describe the process-specific capabilities using a six-axis robot: gravity vector g, normal vector n of the build plate, build direction b – the normal vector of the stratified layers, the orientation of the extrusion axis e and the orientation of the print bed with respect to n and g. Additionally, there are two velocity vectors – linear velocity of the nozzle υ and the angular velocity of the nozzle ω. While υ is essential for all types of FDM processes, it can further be altered by the IR kinematic. However, ω is a unique capability of the IR.

With these parameters, angles can be introduced, which will be further used to describe new process possibilities. $\gamma = 180° - \angle gn$ introduces the angle of the print bed relative to the plummet. $\gamma = 0°$ describes the horizontal orientation of the print bed applied in conventional AM machines. For conventional FDM systems equipped with three linear axes, b and n are collinear. This makes the 2½D layering and motion planning approach possible. Using the IR, the additional rotational degrees of freedom can be used to orient the vectors to each other. Therefore, the layer angle α describes the significant orientation of the build plane with respect to the normal of n and b: $\alpha = \angle nb$. Hence, orienting the build direction b results in the elimination of support structures. If e is tilted from the build direction b, cross-section of the deposited threads changes, thus influencing strength. It is also plausible, that fusion between prior layers is altered when tilting the nozzle axis [10]. This introduces the nozzle angle: $\beta = \angle e\upsilon$.

By facilitating the orientation between the proposed kinematic factors, it is possible to develop new layering strategies and modelling patterns unique to a 6DOF system [8, 11]. This influences the FDM-specific process features of melting, extrusion, deposition, fusion with the prior layer, solidification, and adhesion to print bed. By applying the IR kinematics to adapt the deposition and part modelling strategy, the process approach offers the possibility to further control and optimize mechanical properties such as tensile strength and dimensional accuracy. Hence, a new modelling strategy could take into account the specific part design and load scenario, similar to the method of [12], optimizing crack propagation.

B. Defining Accuracy of an Industrial Robot

Besides the influences of the newly identified parameters, the commissioning of a six-axis kinematic itself needs to be considered. This includes robot-specific issues like accuracy of trajectory, singularity, and self-collision. Speed, strength, and endurance are the main characteristics of IRs which allow their classical applications such as welding or lifting heavy parts in vehicle assembly. Despite advanced calibration methods, the positioning accuracy of robots is still insufficient for many subtractive manufacturing methods like lathing or drilling.

Many influencing variables spoil accuracy, therefore ISO 9283 [13] standardizes performance characteristics and defines performance criteria for IRs and their determination methods. The most important static parameters for a general use of IRs are accuracy of pose (AP) and repeatability of pose (RP). They quantify the differences which occur between a command and attained pose, and the fluctuations in the attained poses for a series of repeat visits to a command pose. However, for AM applications, dynamic properties play a dominant role. The most important parameters, when considering the dynamic motion behavior, are the path accuracy (AT) and path repeatability (RT). AT characterizes the ability of an IR to move its mechanical interface along the command path repeated several times. RT expresses the closeness of the agreement between the attained paths for the same command path repeated several times. Hence, these quantities are a direct measure of the deviation with which a robot can move a tool along a given contour. For example, RT determines the tolerances for beam cutting or welding. The Tool Center Point (TCP) (for FDM – the extrusion nozzle tip mounted to the robot flange) must be positioned and guided with sufficient accuracy. Here classic IRs can reach their limits, especially when the nozzle diameter decreases. For current research, the industrial robot KUKA KR16-2 is used. According to the technical documentation, the accuracy values are: AP = ±0.7 mm; RP = ±0.05 mm; AT = ±0.9 mm (for linear moves at 1m/s); RT = ±0.2 mm (for linear moves at 1m/s). These values suggest working with larger nozzle diameters to ensure bonding between the stratified layers.

To achieve the desired mobility to create form-fit joints, robots with serial kinematics are required, having powerful drives to compensate for the dynamic forces. The positive effect on the IR rigidity is at the expense of absolute position accuracy. Also, slower printing speeds should be considered, as this benefits dynamic accuracy.

C. Programming Method for IRs

Depending on the application of the IR, various online and offline programming methods are available, and are reviewed in [14]. The offline simulation approach of the IR movements offers risk-free collision check of long build-time parts and the possibility to compare different nozzle diameters with each other with little modification effort, and accessibility and cycle time studies can be carried out realistically. Therefore, robot offline simulation environment (ROSE) was used for the ARMS.

III. Developing Requirements for 6DOF AM System

A. Selecting the AM Basic Procedure

No machines or processes were found in the market and patent search that could produce a form-fit connection using AM. Therefore, the fundamental question has to be posed, on which existing AM process can be built on, in order to develop a test system.

The AM processes are divided according to [15] by the aggregate state of the starting material, then by the physical mechanism, from which a process is derived. Reference [16] sorts AM process by the dimensions and number of sources to draw the desired shape and the raw material.

On this basis, extrusion, powder bed and polymerization processes were examined for their suitability to generate a

form fit on or around an existing part. The starting material, be it filament, powder or resin, must be transported into and onto an undercut. If using a powder, it would not be possible to use the laser to conduct the thermal energy directly to the undercut without melting the intermediary powder. The current coating process also leads to a collision with the object in the powder. The same applies to the stereolithographic process where the UV light does not have direct access to the body without illuminating unwanted areas of the bath. It becomes clear that the distance between the surface of the existing structure and the exit point of the process energy to the starting material must be very small. Thus, the extrusion processes were further examined regarding their suitability.

Polylactide (PLA) is chosen as the filament material. Due to its low glass transition temperature of $T_G = 60$ °, it can be processed without a heated print space, keeping the area of investigation as small as possible.

B. Layer Strategies

Six layer strategies have been developed which can create a form-fit joint, shown in Fig. 2:

- Strategy 1: Closing the hole by bodies with negative overhang.
- Strategy 2: Production of a sheath sleeve with remaining overhang.
- Strategy 3: Use of a temporary printing plate.
- Strategy 4: Use of a printing plate in the end product.
- Strategy 5: Fabrication of a contact bridge with subsequent lateral extrusion.
- Strategy 6: Using 45 °-layer angle to close hole with subsequent print.

Care has been given to generate as few new process parameters as possible in order to keep the investigation area as small as possible. All layer strategies generate new parameters that do not occur in the classic FDM process:

- Surface roughness of the existing part – R_z;
- Distance between drill hole edge and outer edge of the print – x;
- Overhang angle – ε;
- Temperature of the front surface of the AM body on which the first layer of the next body is generated – T_I;
- Layer angle α. If x is to be kept as small as possible, the hot end can be designed narrowly, encountering mechanical restrictions quickly. Alternatively, the layers can no longer be printed parallel to the printing plate but must be tilted. The extruder tip is extended and positioned at an angle to the circumferential surface. Thus, two additional rotational degrees of freedom are required. With strategies 2 and 5, a layer angle $\alpha > 0$ °is necessary.

Considering these layer strategies, it becomes clear that more than the translational DOF are necessary. Also considering that the extrusion-based process is best suited for building form-fit AM parts it becomes obvious to use an industrial robot. The availability, documented accuracies and the support of the IR manufacturer, further encourage the decision.

IV. Hardware Implementation

The newly developed and commissioned test system is shown in Fig. 3 and schematically depicted in Fig. 4. It is able to build form-fit joints on the basis of strategies 1 to 6 and to measure the effects of the new parameters α, β and γ. Core component is the KUKA KR-16-2 six-axis robot with a KRC4 control. The robot arm allows for a payload of 16 kg at the mounting flange. The flange can be positioned in all 6 DOF and reaches a work envelope volume of about 14.5 m^3.

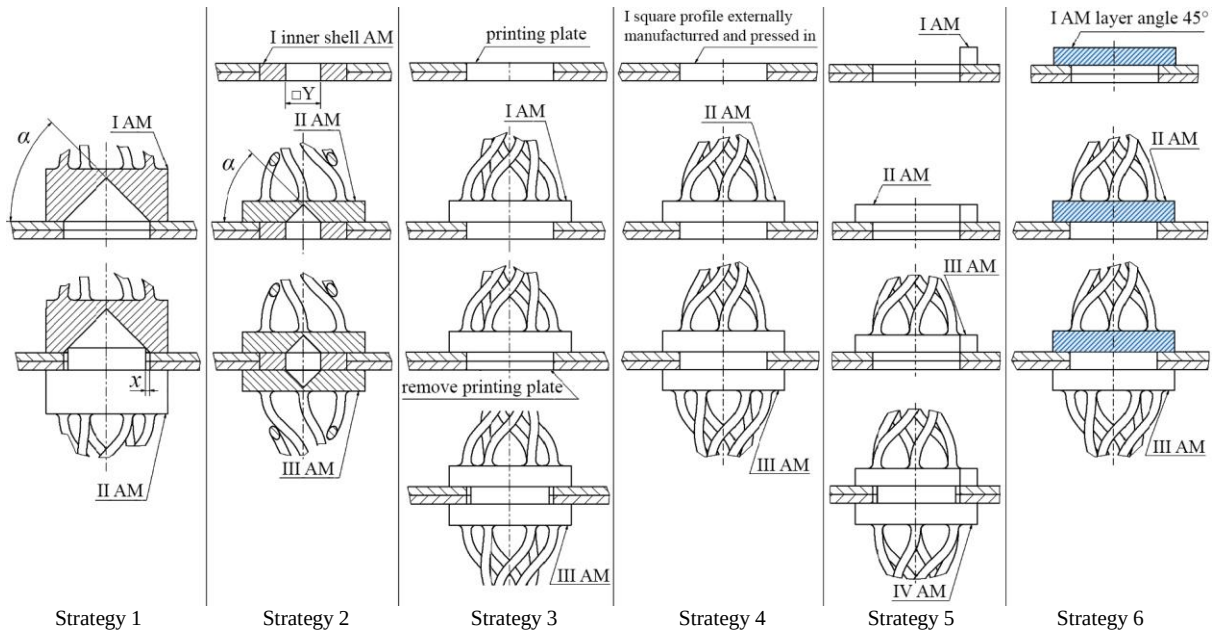

Figure 2. Layer strategies for creating form-fit joints using FDM.

(a)

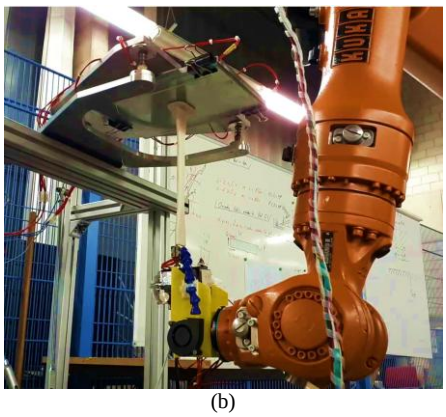

(b)

Figure 3. Commissioned ARMS:
(a) general view; (b) print a test specimen with $\gamma = 180°$.

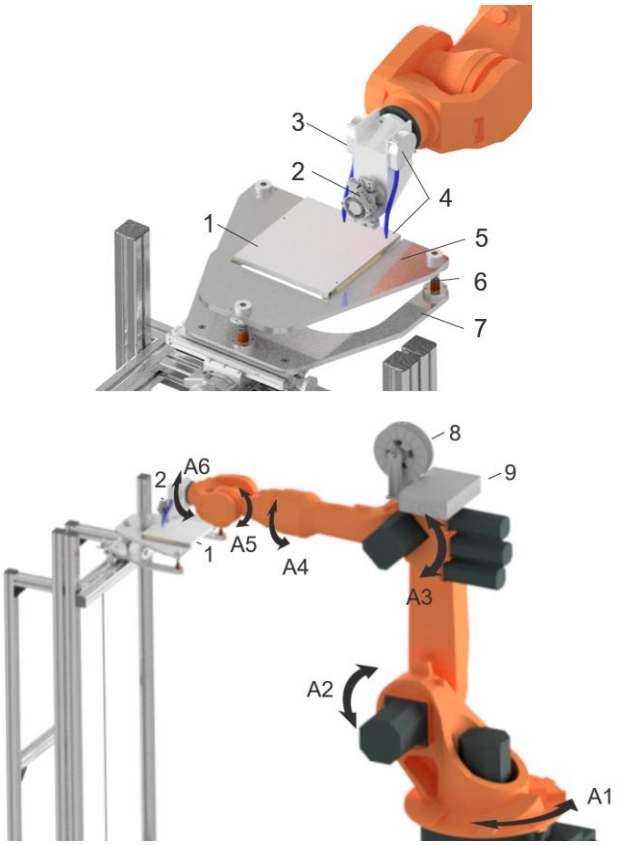

Figure 4. Schematic visualization of the ARMS:
A1-A6 – robot axes; 1 – print bed; 2 – extruder; 3 – connector; 4 – radial fans with cooling hose; 5 – upper fork; 6 – three-point support; 7 – lower fork; 8 – filament spool; 9 – control box.

A E3D-Online Ltd. Titan Aero Kit (hot end and extruder) is connected to the robot flange by a FDM printed connector. The heat block has been rebuilt to use two PID controlled 30W heating capsules instead of one, to ensure that enough thermal energy is provided for higher extrusion speeds and for using tougher filament materials for further investigations (Fig. 5).

A heat brake is positioned between the heat block and the stepper motor powering the extruder serving two purposes: The notch in the middle of the shell surface significantly reduces thermal conductivity from the heat block to the stepper motor. Also, in case of a collision, the notch serves as predetermined breaking point to prevent damage to the extruder, robot or print bed and print pedestal.

The print bed has been built to allow printing tensile specimens from the top, bottom and side, making it possible to isolate γ for 0 °, 90 °, 180 °(Fig. 3 and 4). The pedestal is built using common 40×40 mm aluminum profiles. The first pedestal was built without spring mounts, resulting in inconsistent quality specimens with poor surface quality. Therefore, the print bed is mounted by three-point supports. Each support is spring mounted to yield to the process forces, thus increasing part quality and lowering the risk of damage in case of collision. The lower fork as well as the pedestal sit on anti-vibration mats, further dampening the print bed. Although the force exerted on the upper layer by the heated nozzle is very low, minor impacts still exist due to blobs on the upper cooled off layer and turning inaccuracies. As the nozzle takes off and still has some material left, it may create a minor blob. When the heated nozzle hits such a blob, there is not enough time for the nozzle to melt it, thus resulting a minor shock, creating visible vibrations going through the whole pedestal. The mounts allow a vertical displacement of ±5 mm for calibration.

The print bed dimensions reach up to 340×170×10 mm. They were chosen in order to print three specimens modified from the ISO 527-1a standard [17]. The bed is also heated by PID controlled 6×40 W capsules positioned at the sides of the bed to ensure constant temperature of 65 ° (indicated by wires in Fig. 3). A print-bed containing a square 50 mm hole to conduct feasibility test for strategies mentioned in Fig. 2 was also built.

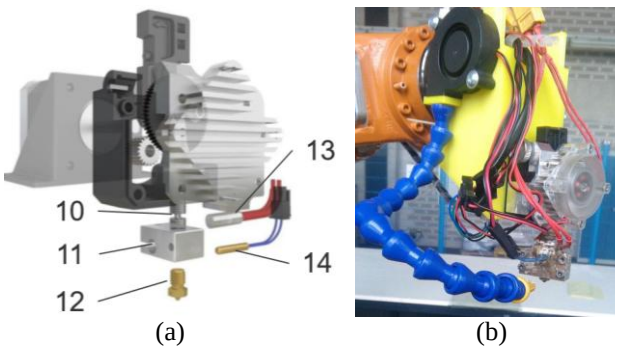

(a) (b)

Figure 5. Implementing FDM extruder for test stand:
a) factory extruder: 1 – heat brake; 2 – heat block; 3 – nozzle; 4 – heating capsule; 5 – thermistor;
b) implemented extruder for IR with modified heat block.

V. Software Implementation

A. General Dataflow

The dataflow of the ARMS, from the idea to the physical part, is portrayed in Fig. 6. The first steps are similar to the 2½D approach (reviewed in [18]) until the G-Code is generated. As the G-Code is rooted in machine tool communication and cannot be interpreted by a robot control, additional tool is necessary to convert and alter the G-Code to KUKA robot language (KRL). Additionally, as safety concerns increase, when working with a robot, the generated code should be checked for collisions. RoboDK© was chosen as the robot offline simulation environment (ROSE), as all criteria are fulfilled, and educational discounts were offered. Furthermore, additional important tools like positioning objects in space and a large documentation are available.

After RoboDK generates KRL-code using a modified post-processor (PP), it is being send to the internal storage of the KRC4 control unit. The extrusion advance values are being send to an EtherCAT Shield for an Arduino microcontroller, which controls the stepper motor driver of the filament extruder, heat elements, and thermistor.

A second microcontroller, not mentioned in Fig. 6, controls the temperature of the print bed independent of the KRL-code.

B. G-Code to Robot Language Translation and Application

Robot moves are distinguished between two types:

- Point to Point (PTP): The robot guides the TCP along the fastest path to the end point. The fastest path is generally not the shortest one and is thus not a straight line. Since the motions of the robot axes are rotational, curved paths can be executed faster than straight paths. However, the exact path of the motion cannot be accurately predicted and is not used for the print process;
- Controlled Path (CP): During CP movement, the TCP moves along mathematically defined path which may be in the form of straight line, circle, or spline in space.

The G-Code outputs only linear commands for printing movements, which the PP translates to CP linear moves. If the robot is forced to touch every point defined through a line move, the TCP would have to come to a full stop. Since the acceleration of a robot is much slower than the linear drives of a conventional FDM-Printer, heavy over-extrusion is the result, as seen in Fig. 7(a). To remedy this, approximation is activated. This feature allows the robot control to deviate from the defined path to create tangential transitions between the target points, Fig. 7(b). This results in a nearly constant TCP velocity as schematically shown in Fig. 7(c). The approximated controlled path is still mathematically defined and can thus be safely used for printing moves. This change in dataflow made it necessary to revisit and redevelop the synchronization between IR-movement and extrusion timing, the amount including mass flux and retraction programming approaches.

The values for the beginning of approximation were set to 0 mm and the maximum number of motion instructions that the robot controller can calculate and plan in advance were set to 1. This forces the robot control to create as small deviations from the target value (P2 in Fig. 7(b)) as possible.

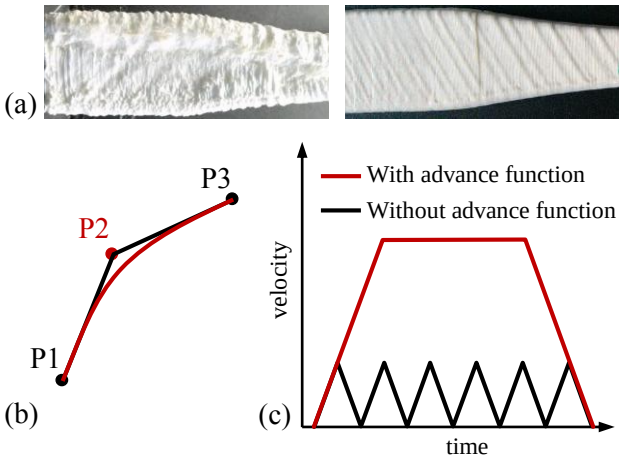

Figure 7. Effect of approximation: (a) Specimen build without and with approximation; (b) Result of approximation on deviation from line moves; (c) Velocity without and with approximation.

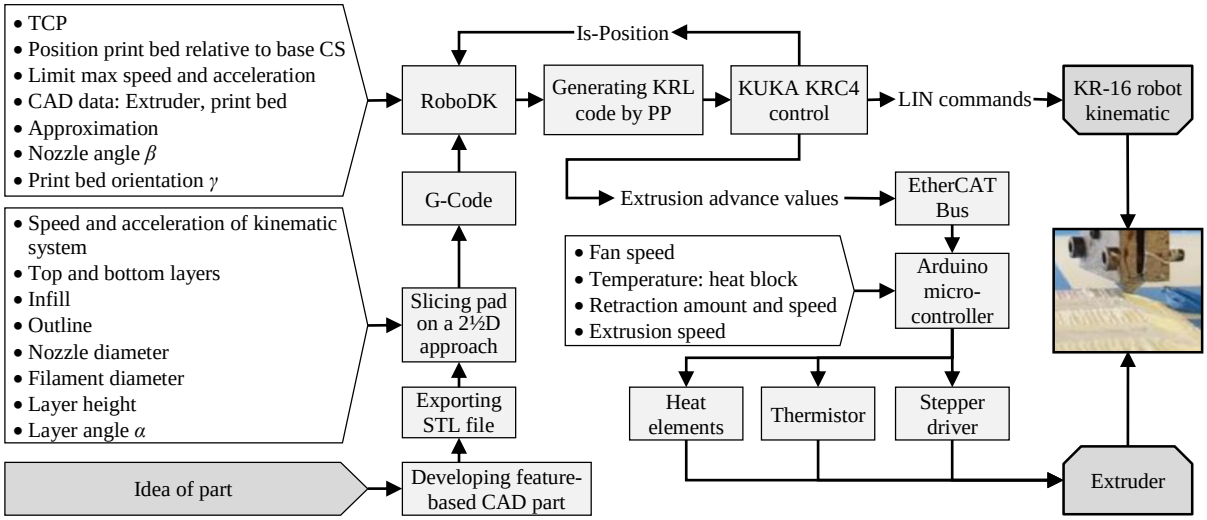

Figure 6. Dataflow of the test stand.

On the downside, these approximation settings alter the geometry of the outline, creating radiuses where sharp corners are expected. This reduces overlap percentage of the infill to the wall which is important for the internal force flux of the specimen. It can be partially compensated by increasing the outline overlap in the slicer.

C. Coordinate Systems

To successfully process the G-Code based on a 2½D slicer generated data to target position in physical space, several coordinate systems (CS) are necessary. They are shown in Fig. 8 using RoboDK environment:

- Base: Absolute CS, not defined by the user but received from the KUKA Control System;
- Robot Flange: CS to define the position of the robot flange that connects to the extruder; defined by the robot kinematic;
- TCP: Tip of the extruder nozzle, therefore defined by its construction;
- Corner CS for calibrating the position of the physical print bed in space;
- Center CS of the print bed which the slicer origin CS (shown in Fig. 9(a)) is aligned with.

In the 2½D slicer Simplify3D©, the origin CS of the build space is positioned on top of the print bed and close to the center – Fig. 8. As the G-Code is imported, a CS for the print bed is necessary to position all movements to the real print bed. Therefore, the exact position of the print bed needs to be communicated to the ROSE. A corner of the physical print bed with its rectangular shape proved ideal for measuring its position relative to the base CS. RoboDK allows creating reference frames based on physical structures inside the working space of the robot. To define the Corner CS of the print bed, the physical extruder nozzle is being moved to three points on the print bed surface, one being the origin at its bottom left corner. If a desired point of the bed is reached, the current position of all six axes is read out to define a point in space. This is being repeated until all three points are measured to define a CS.

VI. Modifying Angles

Fig. 9 shows the procedure when the layer angle α needs to be isolated. First, the specimen is rotated around a desired axis inside the 2½D slicer – (a). No supports are generated. After the G-Code is saved, it is imported into the ROSE and referenced to the print CS – (b). In a last step, the print bed CS is tilted by -α, thus aligning the specimen back to the horizontal plane – (c).

Although it is mechanically possible to use a conventional FDM system to build the specimens seen in Fig. 9(c), the advantages become more apparent when printing an L-shaped body without support structures using 6DOF AM, by changing α from 0 °to 90 °.

The nozzle angle β on a plane is defined by the direction of where the nozzle is moving as seen in Fig. 1. Therefore, if the value is <90 °the melt is being pushed in front of the nozzle, if the value is >90 °the melt is dragged behind. To observe the effects of changing the β angle between the nozzle axis relative to the layers, the CS of the TCP can be tilted using offset values.

Inside the ROSE, the tool can be directed with a "minimum tool orientation change" algorithm. This means that the extruder turns along the *z*-axis as little as possible along the toolpath. This option is suitable for general printing operations. If the melt needs to be either pulled behind or pushed in front of the nozzle, the "tool orientation following the toolpath" algorithm becomes necessary. This is one of the algorithms used for cutting applications, as it tries to keep the robot flange in a desired angle to the toolpath. However, it has been proven difficult to keep the nozzle angle constant in one plane for larger parts. Fig. 10 shows first results of printing tensile test specimens modifying α and β, and using the described algorithm – in case (c).

The angle of the print bed γ can be investigated by printing on the downside of the bed or tilting the bed. This can be simulated by recalibrating the corner CS of the print after turning the physical bed to the desired position. The pedestal was built, so that overhead printing is possible, without turning the bed to γ = 180 °, as seen in Fig. 3 (b).

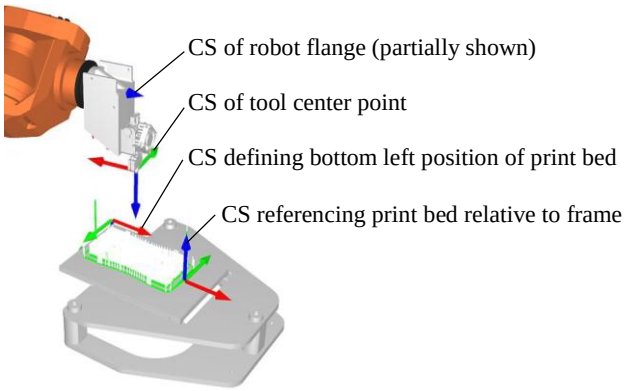

Figure 8. Coordinate systems in robot offline simulation environment.

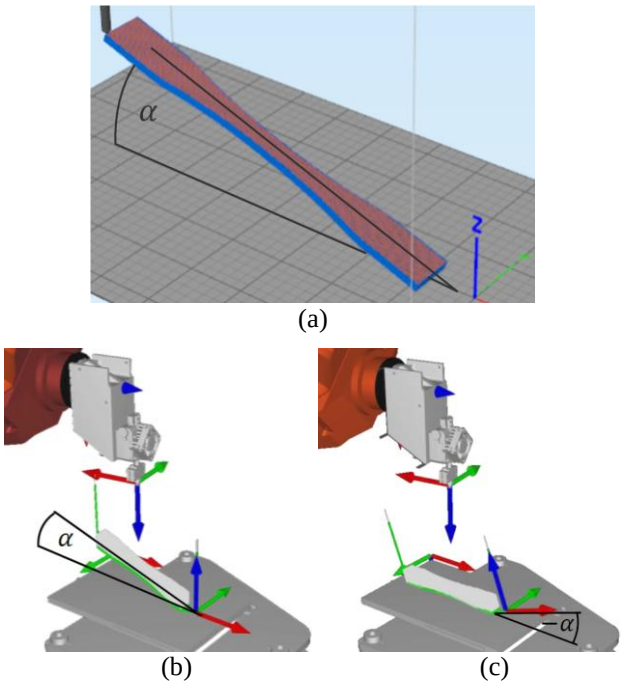

Figure 9. Steps to isolating the layer angle:
(a) tilted specimen in 2½D slicer; (b) imported generate G-Code to ROSE; (c) tilted reference frame.

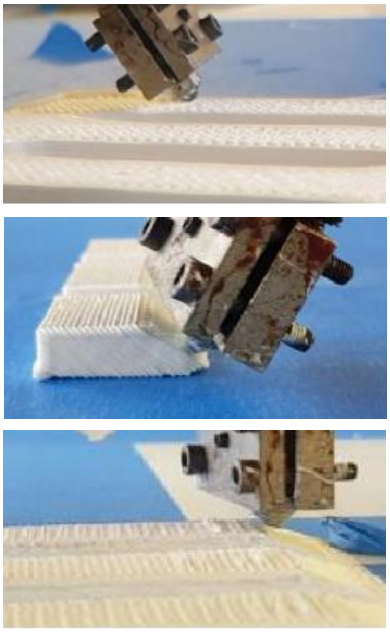

Figure 10. Printing with: a) $\alpha = 0°$, $\beta = 70°$; b) $\alpha = 45°$, $\beta = 90°$; c) $\alpha = 20°$, $\beta = 70°$ using "minimum tool orientation change" algorithm.

VII. Results & Discussion

After all challenges were addressed, different parts and joints were successfully built using the described IR test system – Fig. 11. The purpose of these builds is to benchmark the ARMS regarding process stability of large and small parts (Fig. 11 (a) and (b)). Prior to these, benchmarking parts like calibration cubes and retractions towers readily found in the online AM community were used to calibrate the system regarding retraction settings and mass flux of the extruder. This allowed a feasibility test regarding form-fit joints. Fig. 11 (c) and (d) shows the process of printing a joint connection using strategy 1 shown in Fig.2. The first conically shaped part of the joint was printed on top of the print bed. The bed contains a square 50 mm hole and is oriented to $\gamma = 90°$ (c). Underneath the top part, the printing process of the second part of the form-fit joint onto the undercut from below is shown in (d). This confirms the functionality of the proof of concept to print form-fit joints using an IR.

This possibility establishes the basis for further research and development.

As a next step, it needs to be investigated how α, β, γ and the lower accuracy of trajectory of the IR itself affect strength, stiffness and dimensional accuracy. Also a methodology for determining the quality of the built form-fit joints in comparison with commonly manufactured joints, needs to be developed and evaluated. It has been proven challenging to synchronize robot-movement with the extruder, considering the decreased acceleration and the effect of approximation mentioned. This encourages further optimization, e.g. synchronizing actual acceleration of the IR with the flow-rate of the extruder.

VIII. Conclusion

Following the general goal to produce form-fit joints, an Additive Robot Manufacturing System (ARMS) was successfully developed and commissioned. Although the ability of the current prototype to produce such parts was proved, a lot of additional tasks arise. From one side, improvements are required, especially related to the software solutions for 6DOF printing. From the other side, a lot of research is needed to find the optimal values of the process parameters. In future study we will pay a special attention on the influence of the layer-, tilt-, and print-bed angles α, β and γ on the strength and deformational behavior of the produced parts.

Conflict of Interest

The authors declare no conflict of interest.

Author Contributions

Maurice Schwicker together with students of the University of Applied Sciences Kaiserslautern, developed and commissioned the test stand and conducted first experiments. Nikolay Nikolov and Maurice Schwicker analyzed the data and wrote the paper; all authors had approved the final version.

Acknowledgment

The authors would like to thank the Research and Innovation Committee of the University of Applied Sciences Kaiserslautern for the financial support, and the ITWM Fraunhofer Institute for providing the robot.

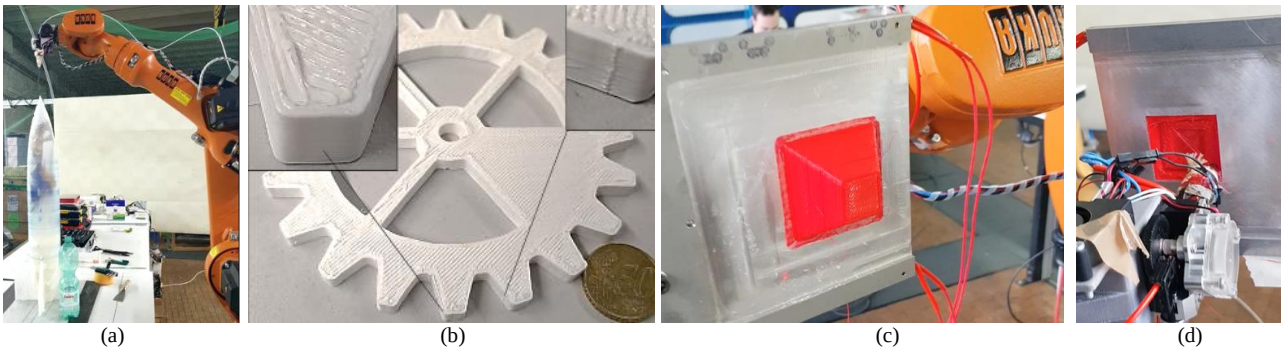

Figure 11. Parts produced using ARMS: a) 1000 mm rocket shell – hollow print using vase-mode, print-speed 60mm/s, nozzle diameter 1mm; b) Gear with diameter 115 mm, build with 0.4 mm nozzle diameter at 30 mm/s; c, d) Building a form-fit joint using strategy 1 at $\gamma = 90°$ (top & bottom view).

REFERENCES

[1] *FDM for End-Use Parts : Tips and Techniques for Optimization – Technical Application Guide*, Stratasys, TAG 30-01, 2011.

[2] M. S. Alsoufi and A. E. Elsayed, "Surface roughness quality and dimensional accuracy – A comprehensive analysis of 100% infill printed parts fabricated by a personal/desktop cost-effective FDM 3D printer," *Mater. Sci. Appl.*, vol. 09, no. 01, pp. 11-40, 2018.

[3] S. Ahn, M. Montero, D. Odell, S. Roundy, and P. K. Wright, "Anisotropic material properties of fused deposition modeling ABS," *Rapid Prototyp. J.*, vol. 8, no. 4, pp. 248-257, Jan. 2002.

[4] H. C. Song, N. Ray, D. Sokolov, and S. Lefebvre, "Anti-aliasing for fused filament deposition," *Comput. Des.*, vol. 89, pp. 25-34, 2017.

[5] J. R. Kubalak *et al.*, "Design and realization of a 6 degree of freedom robotic extrusion platform," in *Solid Freeform Fabrication 2016: Proceedings of the 27th Annual International Solid Freeform Fabrication Symposium – An Additive Manufacturing Conference, SFF 2016*, 2016, pp. 1314-1332.

[6] I. Ishak, J. Fisher, and P. Larochelle, "Robot arm platform for rapid prototyping: Concept," in *Proc. 2015 Florida Conference on Recent Advances in Robotics, FCRAR 2015*, 2015.

[7] F. Wulle, D. Coupek, F. Schäffner, A. Verl, F. Oberhofer, and T. Maier, "Workpiece and machine design in additive manufacturing for multi-axis Fused Deposition Modeling," *Procedia CIRP*, vol. 60, pp. 229-234, 2017.

[8] P. M. Bhatt, R. K. Malhan, A. V. Shembekar, Y. J. Yoon, and S. K. Gupta, "Expanding capabilities of additive manufacturing through use of robotics technologies: A survey," *Additive Manufacturing*, vol. 31., 2020.

[9] M. Rieger, B. Johnen, and B. Kuhlenkötter, "Analysis and development of the fused layer manufacturing process using industrial robots," in *Proc. 47th International Symposium on Robotics, ISR 2016*, 2016, pp. 1-8.

[10] D. Ahlers, F. Wasserfall, N. Hendrich, and J. Zhang, "3D printing of nonplanar layers for smooth surface generation," in *Proc. IEEE 15th International Conference on Automation Science and Engineering (CASE)*, pp. 1737-1743, 2019.

[11] C. Dai, C. C. L. Wang, C. Wu, S. Lefebvre, G. Fang, and Y. J. Liu, "Support-free volume printing by multi-axis motion," *ACM Trans. Graph.*, vol. 37, no. 4, p. 13, 2018.

[12] J. Gardan, A. Makke, and N. Recho, "A method to improve the fracture toughness using 3D printing by extrusion deposition," *Procedia Struct. Integr.*, vol. 2, pp. 144-151, 2016.

[13] Manipulating industrial robots – Performance criteria and related test methods, ISO Strandard 9283:2003.

[14] Z. Pan, J. Polden, N. Larkin, S. Van Duin, and J. Norrish, "Recent progress on programming methods for industrial robots," *Robotics and Computer-Integrated Manufacturing*, vol. 28, no. 2. pp. 87-94, 2012.

[15] A. Gebhardt, J. Hötter, *Additive Manufacturing*, Aachen: Carl Hanser Fachbuchverlag, 2016, ch. 2.5.

[16] I. Gibson, D. Rosen, B. Stucker, and M. Khorasani, *Additive Manufacturing Technologies*, 3rd ed. Springer, 2021, ch. 2.6.

[17] Plastics – Determination of tensile properties – Part 2: Test conditions for moulding and extrusion plastics, ISO Standard 527-2:2019.

[18] R. D. Dandagwhal, A. M. Nikalje, and E. R. Deore, "Effect of process parameters on additively manufactured parts using FDM process & material selection: A review," in *Proc. IOP Conf. Ser. Mater. Sci. Eng.*, vol. 810, no. 1, p. 012031, Apr. 2020.

Maurice Schwicker was born in Wiesbaden, Germany. He has Diploma (FH) and M. Eng. degrees in mechanical engineering from the University of Applied Sciences RheinMain and Kaiserslautern. He is currently a research fellow at the University of Applied Sciences Kaiserslautern, Department of Applied Engineering Sciences. His research interests include Additive Manufacturing with a focus on Fused Deposition Modeling using Robotics and Selective Laser Sintering of polymers.

Nikolay Nikolov was born in Sofia, Bulgaria. He has B.S., M.S, and Ph.D. degrees in mechanical engineering from Technical University of Sofia. He is currently associated professor in Technical University of Sofia, Department of Mechanics. His research interests include Strength of Materials, strength-related numerical modeling, strength- and deformational analysis of details and structures. His current research projects include influence of additive manufacturing process parameters on strength, and influence of corrosion on strength.